

# Synthetic Spectra of Hydrodynamic Models of Type Ia Supernovae

Peter Nugent<sup>1,2</sup>, E. Baron<sup>2</sup>, David Branch<sup>2</sup>, Adam Fisher<sup>2</sup> and Peter H. Hauschildt<sup>3,4</sup>

Received \_\_\_\_\_; accepted \_\_\_\_\_

arXiv:astro-ph/9612044v1 4 Dec 1996

---

<sup>1</sup>Lawrence Berkeley Laboratory, University of California, 1 Cyclotron Road, Mail Stop 50-232, Berkeley, CA, 94720; penugent@lbl.gov

<sup>2</sup>Dept. of Physics and Astronomy, University of Oklahoma, 440 W. Brooks, Rm 131, Norman, OK 73019-0225; baron,branch,fisher@phyast.nhn.ou.edu

<sup>3</sup>Dept. of Physics and Astronomy, University of Georgia, Athens, GA 30602-2451; yeti@hal.physast.uga.edu

<sup>4</sup>Dept. of Physics and Astronomy, Arizona State University, Tempe, AZ 85287-1504

## ABSTRACT

We present detailed NLTE synthetic spectra of hydrodynamic SNe Ia models. We make no assumptions about the form of the spectrum at the inner boundary. We calculate both Chandrasekhar-mass deflagration models and sub-Chandrasekhar “helium detonators.” Gamma-ray deposition is handled in a simple, accurate manner. We have parameterized the storage of energy that arises from the time dependent deposition of radioactive decay energy in a reasonable manner, that spans the expected range. We find that the Chandrasekhar-mass deflagration model W7 of Nomoto et al. shows good agreement with the observed spectra of SN 1992A and SN 1994D, particularly in the UV, where our models are expected to be most accurate. The sub-Chandrasekhar models do not reproduce the UV deficit observed in normal SNe Ia. They do bear some resemblance to sub-luminous SNe Ia, but the shape of the spectra (i.e. the colors) are opposite to that of the observed ones and the intermediate mass element lines such as Si II, and Ca II are extremely weak, which seems to be a generic difficulty of the models. Although the sub-Chandrasekhar models have a significant helium abundance (unlike Chandrasekhar-mass models), helium lines are not prominent in the spectra near maximum light and thus do not act as a spectral signature for the progenitor.

*Subject headings:* supernovae: general

## 1. Introduction

Type Ia supernovae (SNe Ia) are among the brightest known objects in the universe. Since they form a nearly homogeneous class and simple selection criteria can make the observed dispersion quite small, they are natural cosmological probes (Vaughan et al. 1995). The observed homogeneity has led to a search for a homogeneous progenitor, that would satisfy the requirement of lacking hydrogen. This has led to the assumption that the SNe Ia progenitor involves the explosion of a Chandrasekhar-mass white dwarf. The current status of the search for the identification of the SNe Ia progenitor is reviewed in Branch et al. (1995). Hydrodynamic explosion models have included deflagration models such as the “W7” model of Nomoto, Thielemann, & Yokoi (1984). While this model is somewhat hand-crafted to fit the observed spectra and suffers from an overproduction of neutron rich species, it remains the standard in the field. The “DD” (delayed detonation, Khokhlov 1991a; Woosley 1991) and “PDD” models (Pulsating Delayed Detonation, Khokhlov 1991b) improve the predicted nucleosynthetic yield and gives qualitative agreement with the observed spectra and light curves (Höflich & Khokhlov 1996).

The observation of the super-luminous SN 1991T (Jeffery et al. 1992) and the very sub-luminous SN 1991bg (Filippenko et al. 1992) convincingly showed that the class of SNe Ia is not entirely homogeneous. In attempting to model SNe Ib, Livne & Glasner (1990, 1991) examined a “helium-igniter” where a sub-Chandrasekhar or a Chandrasekhar-mass C/O white dwarf with an accreted helium shell detonates near the center following the detonation of the helium shell. Motivated by observations of SN 1991T and 1991bg as well as other claims for evidence that SNe Ia form a sequence (Phillips 1993; Hamuy et al. 1995) Woosley & Weaver (1994) and Livne & Arnett (1995) investigated the helium-igniter as a realistic model for SNe Ia.

On the face of it helium-igniters have much to recommend them as a plausible

progenitor model of SNe Ia. By varying the initial white dwarf mass such models can produce a range of nickel mass  $M_{\text{Ni}} \approx 0.2 - 1.0 M_{\odot}$ , naturally leading to a sequence of supernovae. Sub-Chandrasekhar models do not suffer from the same neutronization problem that occurs in the C/O deflagration models, and population synthesis studies may produce the progenitors in the requisite quantities (Tutukov, Yungelson, & Iben 1992), although not in old populations (Branch et al. 1995).

On the negative side, the models produce an outer shell of the products of explosive helium burning: helium and  $^{56}\text{Ni}$ ; elements not typically associated with the outer layers of SNe Ia. In addition the light curves are extremely fast (Woosley & Weaver 1994; Höflich & Khokhlov 1996), so in particular, it is not clear that the observed photometric diversity can be reproduced by such models.

Since one of the primary goals of synthetic spectral synthesis is the confrontation of theoretical models with observations, we present the results of synthetic spectrum calculations of the helium igniter models of Woosley & Weaver (1994) and Livne & Arnett (1995). Since this is our first application of our program of synthetic spectral synthesis to hydrodynamical SNe Ia models, we also present the results of the spectral synthesis of the W7 model (Nomoto, Thielemann, & Yokoi 1984).

## 2. Calculations

The calculations are performed using the generalized stellar atmosphere program PHOENIX 7.1 (Hauschildt 1992a,b, 1993; Hauschildt, Baron, & Allard 1996) in generally the same way we have applied it previously to SNe Ia (Nugent et al. 1995a,b), although we have modified the code to allow the treatment of nebular boundary conditions, as well as stratified composition and a full gamma-ray deposition calculation. We have compared

the results of our  $\gamma$ -ray deposition with more detailed calculations and the agreement is excellent (Young & Kumagai 1995, private communication). The boundary conditions make no assumptions about the form of the flux at the inner boundary, but rather impose continuity requirements on the intensity (with correct Lorentz transformations). Thus all of the flux comes from the atmosphere itself, there is no “light bulb” at the center. PHOENIX accurately solves the fully relativistic radiation transport equation along with the non-LTE rate equations (for some ions) while ensuring radiative equilibrium (energy conservation). The following ions were treated in non-LTE in the calculations reported here (the number of levels follows in parenthesis): He I (11), He II (10), Na I (3), Ne I (26), Ca II (87), Mg II (18), C I (228), O I (36), Fe II (617), Co II (255), Ti II (204), S II (85) and Si II (94).

The hydrodynamical models were evolved in time by assuming that the expansion is homologous, i.e. the velocity of any given mass point was held constant. The models were rezoned into 50 mass zones, with roughly a logarithmic spacing in  $\tau_{\text{std}}$ , where  $\tau_{\text{std}}$  is the total extinction optical depth in the continuum at 5000 Å. Care was taken to resolve the density profiles.

In theory, once we choose a time since explosion the model is completely determined. The density structure is specified by the homology transformation, the compositions are fixed (once decay of the radioactive species has been accounted for) and, since we use observed bolometric luminosity as an input parameter, the temperature structure is then completely determined by imposing the condition of radiative equilibrium. We parameterize the luminosity as:

$$L_{\text{bol}} = \eta L_{\gamma}^{\text{abs}},$$

where  $L_{\gamma}^{\text{abs}}$  is the total instantaneous  $\gamma$ -ray luminosity *deposited in the material* and  $\eta$  is a parameter that measures the net amount of energy stored over time by the material. Note that  $\eta$  differs from the parameter  $\alpha$  defined by Arnett and co-workers (Arnett 1982;

Arnett, Branch, & Wheeler 1985) since  $\alpha$  refers to the *total* instantaneous  $\gamma$ -ray luminosity, and instead corresponds to the parameter  $\tilde{Q}$  of Höflich & Khokhlov (1996). [NB: While the definition of  $Q \equiv \alpha$  in Höflich & Khokhlov (1996), in previous papers in their series  $Q$  corresponds to  $\eta$ ]. Höflich & Khokhlov (1996) found  $\eta$  in the range  $0.7 < \eta < 1.8$  for a wide variety of models that they examined, and we have varied  $\eta$  from approximately 0.5 – 2.0. Actually  $\eta$  should be a function of radius, but an accurate calculation of  $\eta$  will require a NLTE, multi-group radiation-hydrodynamical calculation. This procedure accounts for the time-dependent nature of the deposition of radioactive energy in an accurate manner. Given an input luminosity the temperature structure of the models is determined by demanding the modified radiative equilibrium condition:

$$\int \kappa_{\lambda}(B_{\lambda} - J_{\lambda}) d\lambda - \dot{S} = 0,$$

where  $\dot{S}$  is the local instantaneous rate at which  $\gamma$ -ray energy is deposited.

### 3. Results

#### 3.1. Model W7

Figure 1 displays our synthetic spectrum for the W7 model at 20 d past explosion for three choices of  $\eta$ . This is several days after the time of bolometric maximum  $t_{\text{bol}} = 14$  d found by Höflich & Khokhlov (1996) and Khokhlov, Müller, & Höflich (1993) who found  $\eta = 1.3$  at this time. The magnitudes and colors of these models are listed in Table 1. The model strongly resembles observed SNe Ia spectra, showing the defining Si II  $\lambda 6355$  line as well as the  $\lambda 5972$  line, and lines from Ca II, S II, O I, and Fe II. Also, there is the strong UV deficit that is characteristic of SNe Ia spectra. The colors for the  $\eta = 1.0$  20 d model are very similar (on average) to the colors found for normal SNe Ia. The  $\eta = 2.0$  colors are too blue and the  $\eta = 0.8$  are too red, suggesting that the value of  $\eta = 1.3$ , found by Höflich

and collaborators is reasonable.

In addition to the NLTE lines that we treat directly, we must also include  $\approx 2$  million additional lines in LTE. The shape of the spectrum is somewhat sensitive to the constant thermalization parameter  $\epsilon$  that we choose (Nugent et al. 1995a; Baron et al. 1996), where  $\epsilon$  is defined by the source function for LTE metal lines,

$$S_l = (1 - \epsilon) \int \phi_\nu J_\nu d\nu + \epsilon B_\nu(T).$$

Figure 2 compares the spectra for  $\epsilon = (10^{-4}, 0.05, 0.1, 1.0)$ . The UV (where most lines are treated in NLTE) is rather insensitive to the choice of  $\epsilon$ ; however, in the optical, redward of 5000 Å there is a strong dependence on  $\epsilon$ . Based on our previous work and the results of NLTE calculations, we choose  $\epsilon = 0.05 - 0.1$  as our standard range. All the models discussed below have  $\epsilon = 0.1$ .

Figure 3 shows the W7 model at 23 d ( $\eta = 1.3$ ) with an observed spectrum of SN 1992A [taken at 5 days after maximum light (Kirshner et al. 1993)] and at 20 d ( $\eta = 1.0$ ) with an observed spectrum of SN 1994D [at maximum light in the optical and 3 days before maximum in the IR (Meikle et al. 1996)]. The agreement is quite good across the entire range of observed wavelength for each supernova with all of the major (and most of the minor) features present in the synthetic spectra. While fine tuning could no doubt improve the fits, that is not our purpose in this paper. An interesting feature in Figure 3, is that both the observed spectrum for SN 1994D and the synthetic spectra of W7 show a “split” just blueward of the Ca II H&K feature. This is likely due to a blend of Ca II H&K and Si II  $\lambda 3858$ . Kirshner et al. (1993) also noted that the two lines are of nearly equal strength. While the split is prominent in the observed spectrum of SN 1994D, it is clearly absent in the observed spectrum of SN 1992A. We will return to this issue in future work.

Figure 4 shows the time evolution of the W7 model near maximum light. The bolometric magnitudes and colors of the 16 d,  $\eta = 1.1$  and  $\eta = 1.7$  models (see Table 1)

should be compared with the results of Höflich & Khokhlov (1996) who found  $M_{\text{bol}} = -19.56$  and  $B - V = 0.11$  (for  $\eta = 1.3$ ). The bolometric magnitudes bracket the results of Höflich & Khokhlov (1996), while both of the models are somewhat bluer than they found. This is likely due to differences in the treatment of radiation transport (NLTE, 82,000 wavelength points and full line profiles, versus LTE grey transport) and serves as an estimate of the theoretical uncertainty of such calculations.

### 3.2. Sub-Chandrasekhar Models

Figure 5 displays Model 2 of Woosley & Weaver (1994) (WW2) 15 d after explosion for three choices of  $\eta$ . This model is the explosion of an  $0.7 M_{\odot}$  white dwarf that has accreted  $0.2 M_{\odot}$  of helium. Since these models are significantly less massive than W7, they peak earlier and hence it is sensible to examine them at earlier times. Figure 6 is similar to Figure 5, but for Model 4 of Livne & Arnett (1995) (LA4), which is a  $0.7 M_{\odot}$  white dwarf that has accreted  $0.17 M_{\odot}$  of helium. The magnitude and color data for these models can be found in Table 2. The synthetic spectra have less line-blanketing and hence more flux in the UV, than does the W7 model. There is no strong evidence of either He I or He II lines. Although we do not use the Sobolev approximation at all in our calculations, we calculate the Sobolev optical depth of each NLTE line as a convenient diagnostic. The Sobolev optical depth of the He I  $\lambda 5876$  lines is approximately 3 – 4 orders of magnitude weaker than that of the Si II  $\lambda 6355$  line in both sets of models, thus these models are effective at “hiding helium.” It is somewhat surprising that in a model with nearly  $0.2 M_{\odot}$  helium on the outside that no evidence of helium should appear. This seems to be due to the very strong non-thermal ionization and the high UV flux which tends to keep the helium ionized, and/or highly excited, suppressing the strong He I lines. Optical He II lines, particularly  $P_{\alpha}$   $\lambda 4687.8$  and  $P_{\beta}$   $\lambda 3204.5$ , are also not prominent. At earlier times, with higher densities



recombination may populate the He I – II levels, but since the models will also be hotter at those times, it is not clear *a priori* that optical He I – II lines will ever be strong in these models. Understanding the exact suppression mechanism of helium lines will be the subject of future work.

Figure 7 shows the synthetic spectra of the models of WW2 ( $\eta = 1.1$ ) and LA4 ( $\eta = 1.5$ ) at 20 d, compared with the observed spectrum of SN 1994D. Clearly the synthetic spectra bear little resemblance to the observed SN Ia spectrum. The Si II  $\lambda 6355$  line is quite weak and may not extend to high enough velocity. This is a generic problem with sub-Chandrasekhar models. The 15-d WW2 model of Figure 5 does however reproduce the boxy shape of the Ca IR triplet seen in SN 1994D, which may indicate that the calcium is confined to the correct velocity range in the model.

Sub-Chandrasekhar models have been suggested as attractive models for low luminosity SNe Ia such as SN 1991bg. The spectra of this SN Ia [at maximum (Filippenko et al. 1992) in the optical and IUE data in the UV (NASA Astrophysics Data Facility 1991)] along with the spectra of the 20 d models of WW2 ( $\eta = 1.1$ ) and LA4 ( $\eta = 1.5$ ) can be seen in Fig. 8. These models show some resemblance to the observed SN 1991bg spectrum, however, the shape of the spectra from these models is counter to that observed. This behavior is exemplified by the WW2 20 d model with  $\eta = 1.1$  in Table 2 where  $B - V$  is extremely red (0.74), but  $U - B$  is negative (-0.16). The flat spectrum in the UV for these models (signified by a negative  $U - B$ ) is observationally associated with bright SNe Ia such as SN 1991T and SN 1994D, rather than with dim supernovae such as SN 1991bg. In the spectrum of SN 1991bg, the trough near 4000 Å is due to Ti II (Filippenko et al. 1992; Nugent et al. 1995b). In the synthetic spectra this trough is not flat enough to reproduce the observed spectrum of SN 1991bg, most likely because Ti II is confined to a small region in velocity in these models. Also, the calculated Si II and Ca II lines are very weak even

at this epoch. The strength of these lines correlates inversely with the luminosity of the supernova (Nugent et al. 1995b). Weak, dim supernova like SN 1991bg have strong Si II and Ca II lines, whereas powerful, bright SNe such as 1991T, have weak lines, thus a model that hopes to fit SN 1991bg should show prominent Si II and Ca II lines.

Table 3 lists the relative concentration of the four most abundant species at three different velocities for each of the three models that we have examined (the models W7, WW2, and LA4 have  $\eta = 1.0, 1.0, 1.5$ , respectively) at 20 days after explosion. The models have very similar compositions at low velocity, a mixture of highly ionized iron-peak elements and He II. The detonation models have somewhat more He II than does the deflagration W7. In the outer parts, the composition is different. Whereas W7 has singly and doubly ionized intermediate mass elements, the helium igniters have mixtures of neutral and singly ionized helium, and doubly ionized elements just below the iron-peak (calcium and titanium). At very high velocity ( $v > 20000 \text{ km s}^{-1}$ ), the composition of W7 is mostly a mixture of C–O, while the WW2, and LA4 models are dominated by He I – II. As we have already noted the presence of intermediate mass elements at high velocity is required to fit the observed spectra.

In order to further elucidate the differences between W7 and the helium-igniters, Figure 9 compares the temperature and electron density profiles of W7 ( $\eta = 1.0$ ) to WW2 ( $\eta = 1.1$ ) at 20 d. The more massive W7 model has a much steeper electron density profile, and it is cooler on the outside. Figure 10 displays the Sobolev optical depth of the Co II  $^1D - ^3G^o \lambda 2605.2$  line as a function of  $\tau_{\text{std}}$  for the 3 models. While W7 and WW2 display similar Sobolev optical depths in this line at depth, LA4 only has a very small region where this line is optically thick, and, near the surface where the spectrum forms, both WW2 and LA4 are transparent in this line. This is typical for the iron-peak UV lines and it makes it very difficult for the helium-detonation models to display the proper line blanketing in the

UV. It is not that the iron-peak elements are not present, but rather that they are not in the proper ionization/electronic states to create strong line blanketing.

#### 4. Conclusions

We have calculated very detailed NLTE synthetic spectra of hydrodynamical models for SNe Ia. We have used only symmetry considerations at the inner boundary and thus have not had to make any assumptions about the form of the flux there, the spectrum is calculated *ab-initio*. We have used a simple but accurate  $\gamma$ -ray transport algorithm and we have developed a reasonable parameterization of the time dependence of the  $\gamma$ -ray heating that can be compared with and calibrated to sophisticated radiation hydrodynamical calculations as they become available.

The Chandrasekhar-mass deflagration model W7 shows good agreement with observed normal SNe Ia and it is likely that other Chandrasekhar-mass models such as DD or PDD (Khokhlov, Müller, & Höflich 1993) will also show reasonable agreement. While the sub-Chandrasekhar mass “helium igniter” models bear some resemblance to the sub-luminous SNe Ia typified by SN 1991bg the weakness of lines of the intermediate mass elements and the lack of the UV deficit will have to be addressed if these models are to remain as viable contenders for at least some SNe Ia.

We thank Dave Arnett, Ken Nomoto, and Stan Woosley for providing us with their models and for helpful discussions. We also thank Shiomi Kumagai and Tim Young for allowing us to quote their unpublished results and for helpful discussions on gamma-ray deposition. This work was supported in part by NSF grants AST-9417242 and AST-9417102; an IBM SUR grant to the University of Oklahoma; and by NASA grants NAGW-4510, NAGW-2628, and NAGW 5-3067 to Arizona State University. Some of the calculations

presented in this paper were performed at the Cornell Theory Center (CTC), and the San Diego Supercomputer Center (SDSC), supported by the NSF, and at the National Energy Research Supercomputer Center (NERSC), supported by the U.S. DoE. We thank all of these institutions for a generous allocation of computer time.

### References

- Arnett, W. D. 1982, *ApJ*, 253, 785
- Arnett, W. D., Branch, D., & Wheeler, J. C. 1985, *Nature*, 314, 337
- Baron, E., Hauschildt, P. H., Nugent, P., & Branch, D. 1996, *MNRAS*, 283, 297
- Branch, D., Livio, M., Yungelson, L., Boffi, F., & Baron, E. 1995, *PASP*, 107, 1019
- Filippenko, A. V., et al. 1992, *AJ*, 104, 1543
- Hamuy, M., Phillips, M. M., Maza, J., Suntzeff, N. B., Schommer, R. A., & Aviles, R. 1995, *AJ*, 109, 1
- Hauschildt, P. H. 1992a, *JQSRT*, 47, 433
- Hauschildt, P. H. 1992b, *ApJ*, 398, 224
- Hauschildt, P. H. 1993, *JQSRT*, 50, 301
- Hauschildt, P. H., Baron, E., & Allard, F. 1996, *ApJ*, submitted
- Höflich, P., & Khokhlov, A. 1996, *ApJ*, 457, 500
- Jeffery, D., Leibundgut, B., Kirshner, R. P., Benetti, S., Branch, D., & Sonneborn, G. 1992, *ApJ*, 397, 304
- Khokhlov, A. 1991a, *A&A*, 245, 114

- Khokhlov, A. 1991b, *A&A*, 245, L25
- Khokhlov, A., Müller, E., & Höflich, P. 1993, *A&A*, 270, 223
- Kirshner, R. P., et al. 1993, *ApJ*, 415, 589
- Livne, E., & Arnett, W. D. 1995, *ApJ*, 452, 62
- Livne, E., & Glasner, A. S. 1990, *ApJ*, 361, 244
- Livne, E., & Glasner, A. S. 1991, *ApJ*, 370, 272
- Meikle, W. P. S., et al. 1996, in *Proceedings of the NATO ASI Conference on Thermonuclear Supernovae*, R. Ruiz-Lapuente, R. Canal, and J. Isern, editors, Dordrecht: Kluwer
- NASA Astrophysics Data Facility 1991, IUE Archival Data, <http://ndads.gsfc.nasa.gov/>
- Nomoto, K., Thielemann, F.-K., & Yokoi, K. 1984, *ApJ*, 286, 644
- Nugent, P., Baron, E., Hauschildt, P., & Branch, D. 1995a, *ApJ*, 441, L33
- Nugent, P., Phillips, M., Baron, E., Branch, D., & Hauschildt, P. 1995b, *ApJ*, 455, L147
- Phillips, M. M. 1993, *ApJ*, 413, L105
- Tutukov, A., Yungelson, L., & Iben, I. 1992, *ApJ*, 396, 197
- Vaughan, T. E., Branch, D., Miller, D. L., & Perlmutter, S. 1995, *ApJ*, 439, 558
- Woosley, S. E. 1991, in *Gamma-Ray Line Astrophysics*, P. Durouchoux and N. Prantzos, editors, New York: AIP, page 270
- Woosley, S. E., & Weaver, T. A. 1994, *ApJ*, 423, 371

Table 1. Magnitudes and Colors of W7 Models

Time	$\eta$	$M_{\text{Bol}}$	$M_B$	$M_V$	$B - V$	$U - B$
16 d	0.6	-18.48	-18.64	-18.60	-0.04	-0.35
16 d	0.9	-18.85	-18.95	-18.78	-0.18	-0.64
16 d	1.1	-19.10	-19.11	-18.92	-0.19	-0.79
16 d	1.7	-19.61	-19.44	-19.26	-0.17	-0.91
18 d	0.9	-18.70	-18.93	-18.83	-0.10	-0.37
20 d	0.8	-18.51	-18.71	-18.81	0.10	-0.09
20 d	0.9	-18.55	-18.77	-18.83	0.07	-0.12
20 d	1.0	-18.69	-18.93	-18.93	0.00	-0.17
20 d	2.0	-19.45	-19.54	-19.24	-0.30	-0.82
23 d	1.3	-18.75	-18.93	-19.04	0.10	-0.14
25 d	1.5	-18.81	-19.11	-19.08	-0.04	-0.20

Note. —  $M_{\text{Bol}}$ ,  $M_B$ , and  $M_V$  are the bolometric,  $B$  and  $V$  absolute magnitudes of the models respectively.  $B - V$  and  $U - B$  are the associated colors.

Table 2. Magnitudes and Colors of the Sub-Chandrasekhar Models

Model	Time	$\eta$	$M_{\text{Bol}}$	$M_B$	$M_V$	$B - V$	$U - B$
WW2	15 d	0.7	-18.08	-18.04	-18.68	0.64	-0.18
WW2	15 d	1.0	-18.49	-18.72	-18.82	0.10	-0.31
WW2	15 d	1.3	-18.78	-19.13	-18.83	-0.30	-0.46
WW2	15 d	1.6	-18.98	-19.33	-18.85	-0.48	-0.55
WW2	20 d	1.1	-18.22	-18.21	-18.95	0.74	-0.16
WW2	20 d	1.5	-18.51	-18.78	-18.97	0.19	-0.34
WW2	20 d	1.9	-18.80	-19.17	-18.82	-0.36	-0.65
LA4	15 d	0.7	-18.20	-18.30	-18.81	0.52	-0.17
LA4	15 d	1.1	-18.69	-18.99	-18.90	-0.08	-0.43
LA4	15 d	1.7	-19.17	-19.41	-18.91	-0.50	-0.76
LA4	20 d	1.5	-18.60	-18.96	-18.97	0.01	-0.39
LA4	20 d	1.6	-18.66	-19.03	-18.97	-0.07	-0.43
LA4	20 d	2.0	-18.89	-19.29	-18.91	-0.37	-0.60

Note. —  $M_{\text{Bol}}$ ,  $M_B$ , and  $M_V$  are the bolometric,  $B$  and  $V$  absolute magnitudes of the models respectively.  $B - V$  and  $U - B$  are the associated colors.

Table 3. 4 Most Abundant Species for Each Model at 20 Days After Explosion

Model	Velocity (km s <sup>-1</sup> )	Relative Concentration (ppm)			
W7	20,000	C I ( $2 \times 10^5$ )	O II ( $2 \times 10^5$ )	Ne II ( $2 \times 10^4$ )	O I ( $1 \times 10^4$ )
LA4	20,000	He II ( $4 \times 10^5$ )	He I ( $9 \times 10^4$ )	Ti III ( $6 \times 10^3$ )	Ca III ( $4 \times 10^3$ )
WW2	20,000	He II ( $4 \times 10^5$ )	He I ( $2 \times 10^5$ )	Ti III ( $7 \times 10^3$ )	Ca III ( $6 \times 10^3$ )
W7	10,000	Si III ( $1 \times 10^5$ )	Co III ( $7 \times 10^4$ )	S III ( $6 \times 10^4$ )	Ca III ( $3 \times 10^4$ )
LA4	10,000	Si III ( $1 \times 10^5$ )	Co III ( $1 \times 10^5$ )	S III ( $5 \times 10^4$ )	Ni III ( $1 \times 10^4$ )
WW2	10,000	Si III ( $2 \times 10^5$ )	S III ( $1 \times 10^5$ )	Ar II ( $1 \times 10^4$ )	Ca III ( $1 \times 10^4$ )
W7	5,000	Co IV ( $2 \times 10^5$ )	Ni IV ( $7 \times 10^4$ )	Fe IV ( $2 \times 10^4$ )	He II ( $2 \times 10^3$ )
LA4	5,000	Co IV ( $2 \times 10^5$ )	He II ( $7 \times 10^4$ )	Ni IV ( $2 \times 10^4$ )	Fe IV ( $2 \times 10^4$ )
WW2	5,000	Co IV ( $2 \times 10^5$ )	He II ( $3 \times 10^4$ )	Ni IV ( $2 \times 10^4$ )	Fe IV ( $2 \times 10^4$ )

Note. — The relative concentrations by number of the four most abundant species (in parts per million) for a particular zone (labeled by its velocity). The models W7, WW2, and LA4 have  $\eta = 1.0, 1.1, 1.4$ , respectively.



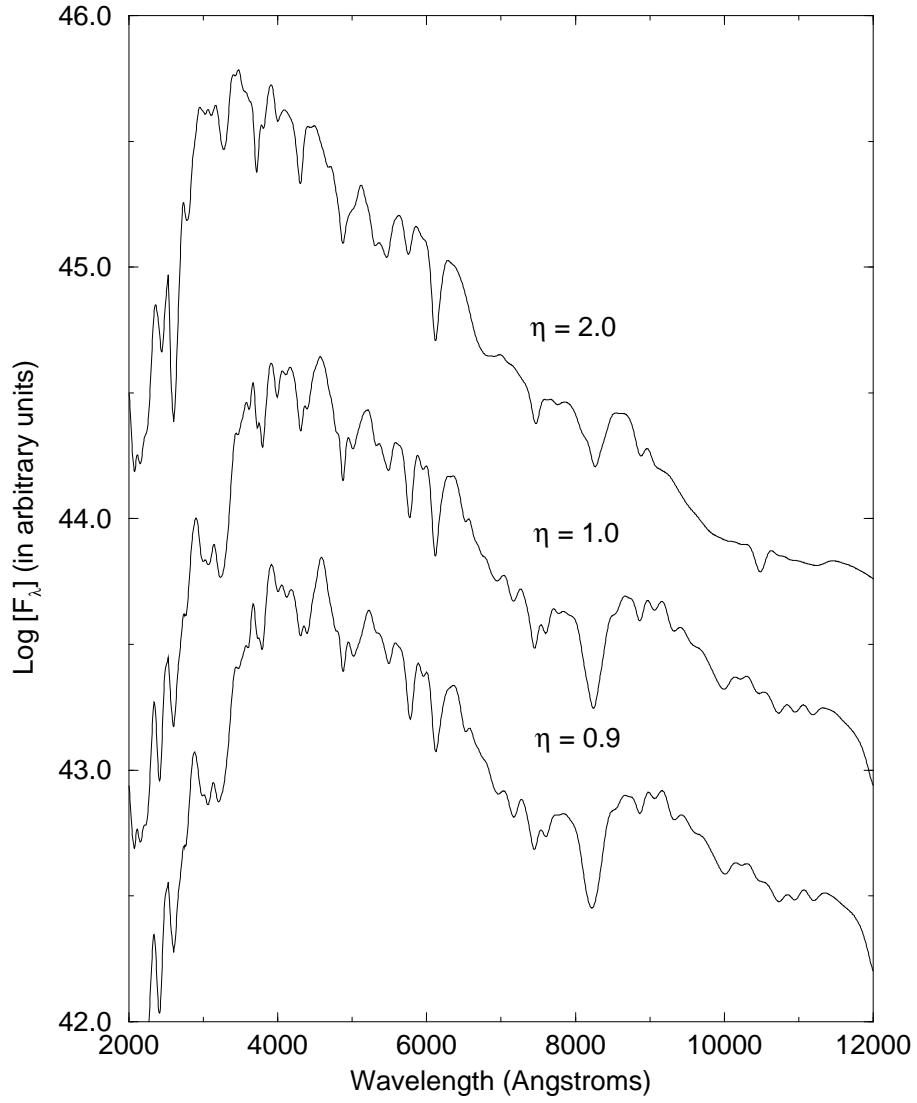


Fig. 1.— The synthetic spectrum for the W7 model at 20 d past explosion for three choices of  $\eta$ .

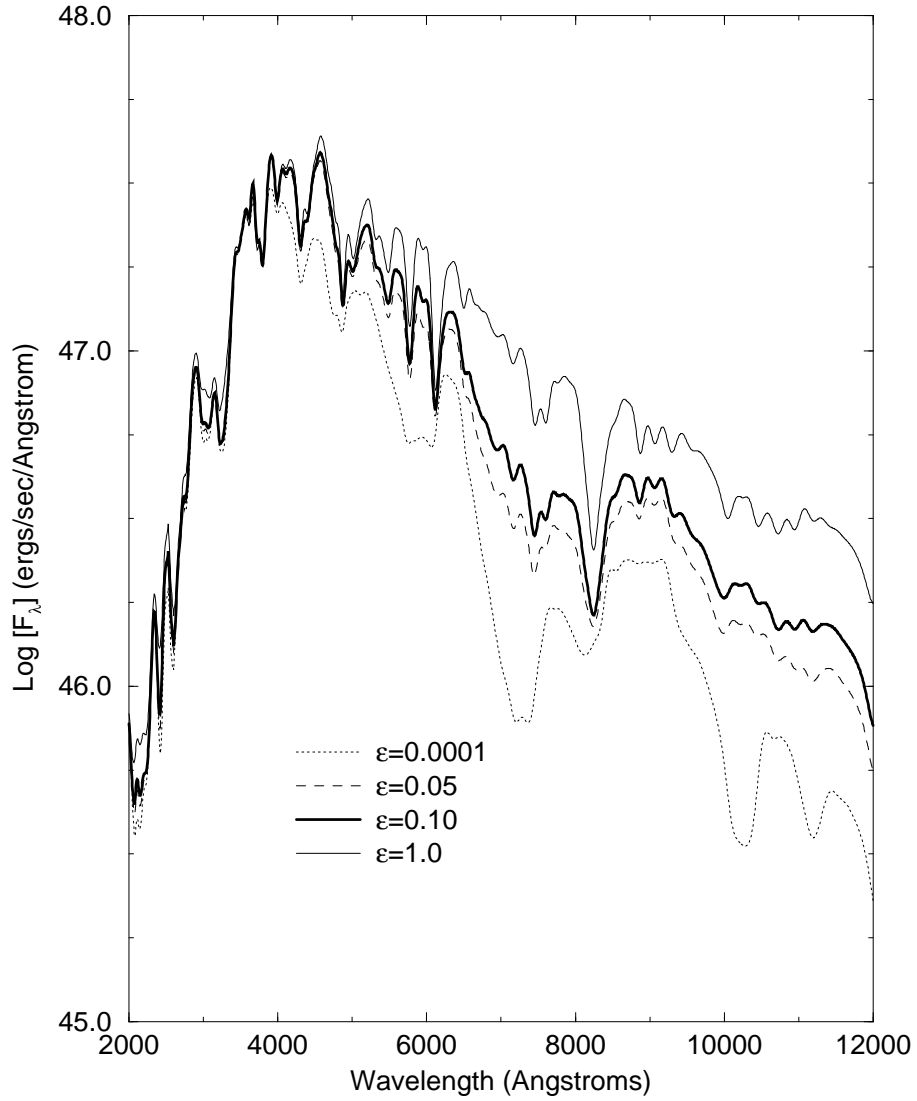


Fig. 2.— The synthetic spectrum for the W7 model at 23 d past explosion ( $\eta = 1.3$ ) for four choices of  $\epsilon$ . The model with  $\epsilon = 0.10$  is in radiative equilibrium and the temperature structure has been held fixed at that structure for all the models displayed.

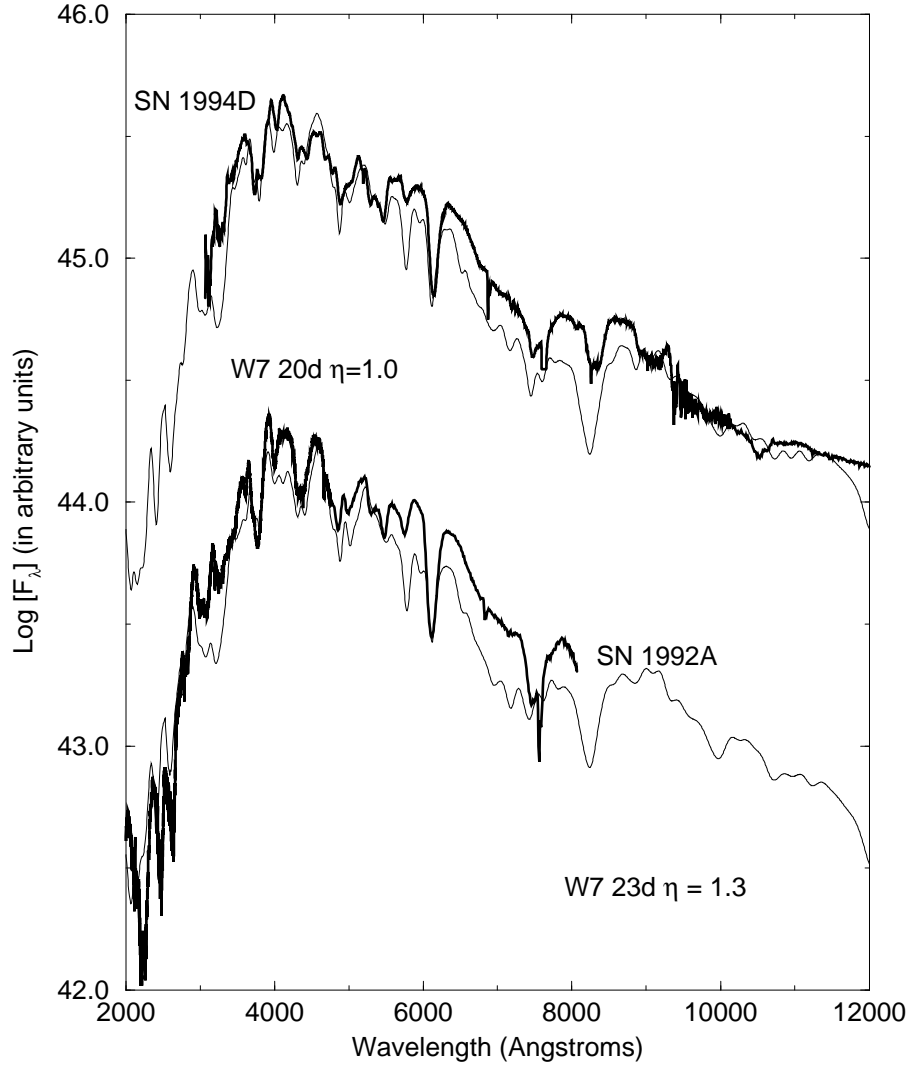


Fig. 3.— The W7 model at 23 d ( $\eta = 1.3$ ) compared with an observed spectrum of SN 1992A [5 days after maximum light (Kirshner et al. 1993)] and at 20 d ( $\eta = 1.0$ ) compared with an observed spectrum of SN 1994D [at maximum light (Meikle et al. 1996)].

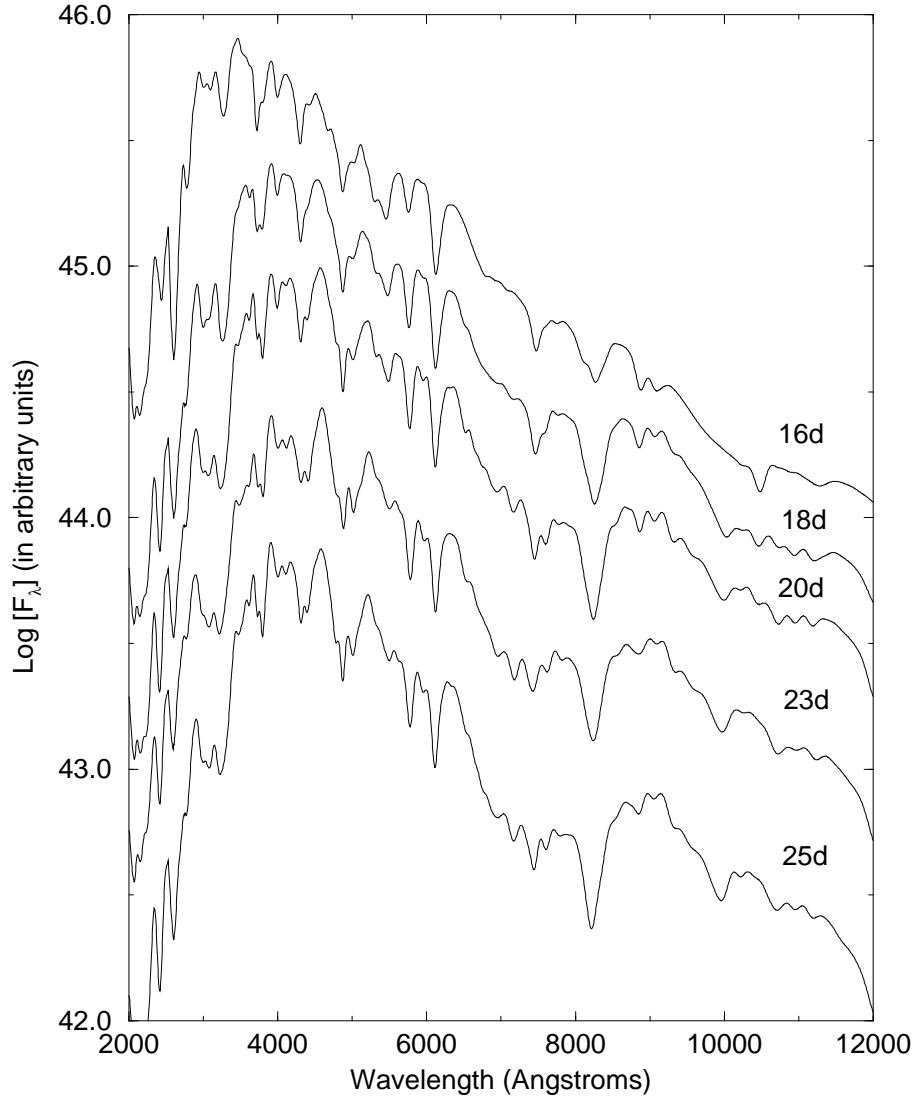


Fig. 4.— The time evolution of the W7 model near maximum light ( $\eta = 1.1, 0.9, 1.0, 1.3, 1.5$  at  $t = 16, 18, 20, 23, 25$  d, respectively).

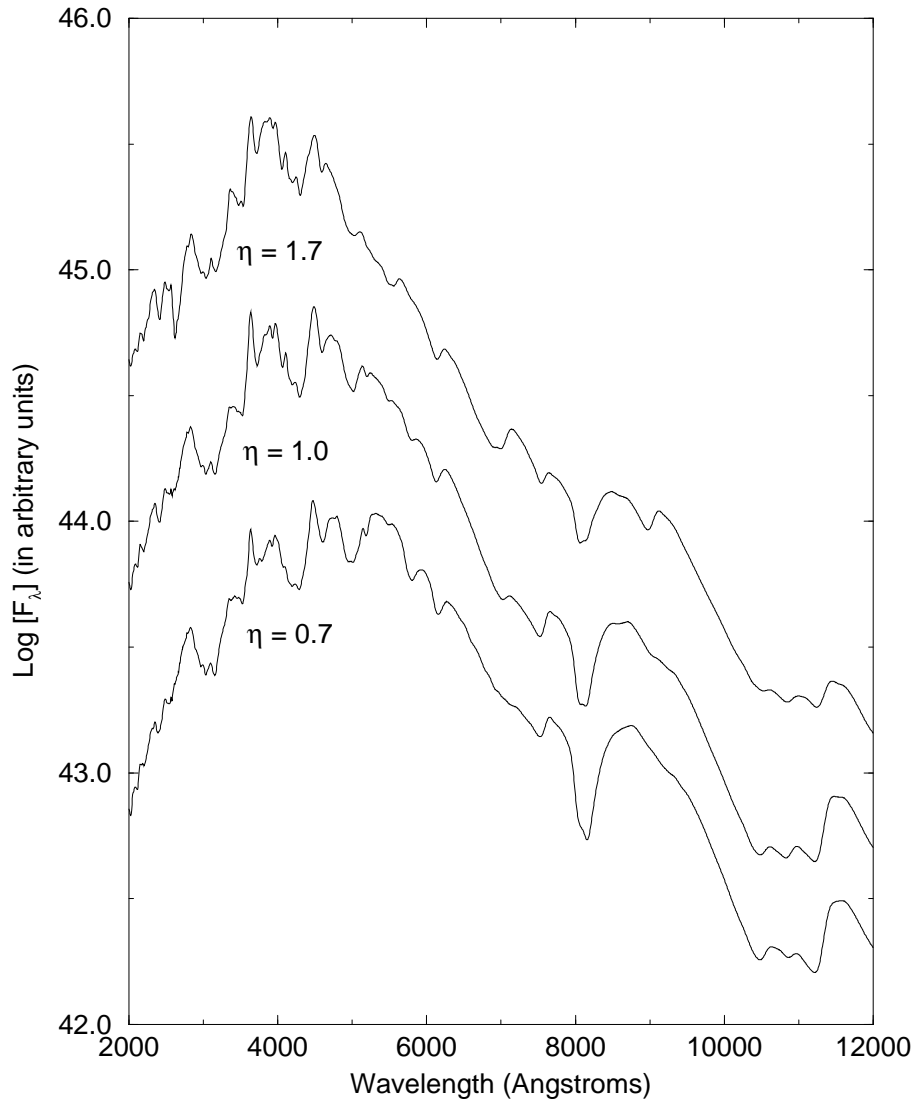


Fig. 5.— Model WW2 15 d after explosion for three choices of  $\eta$ .

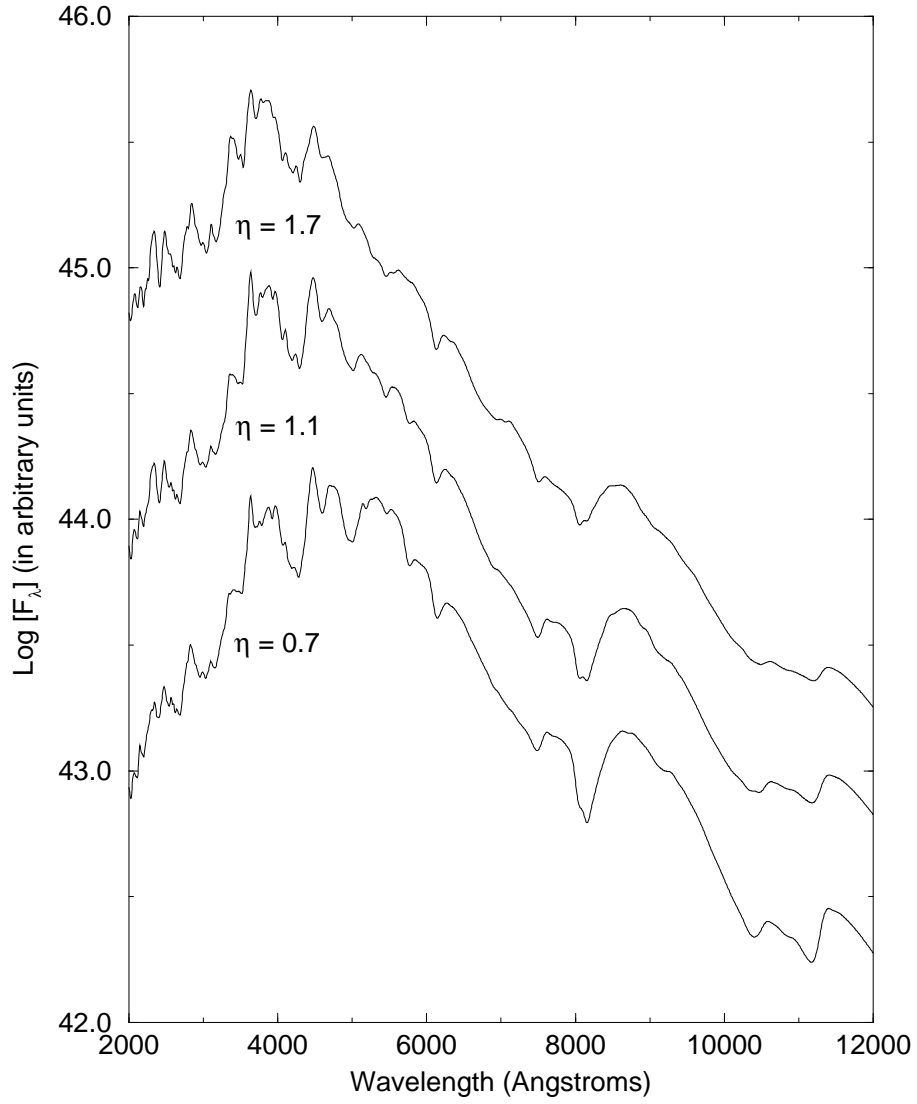


Fig. 6.— Model LA4 15 d after explosion for three choices of  $\eta$ .

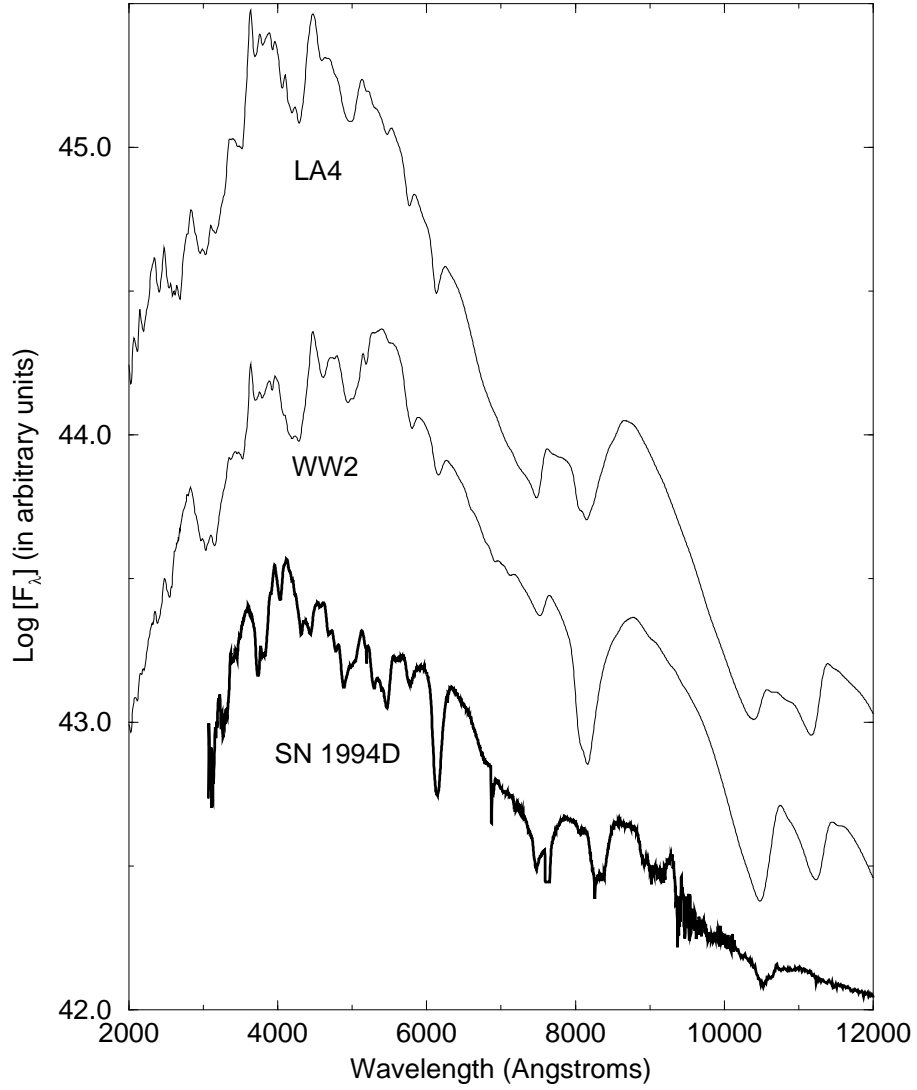


Fig. 7.— The synthetic spectra of WW2 ( $\eta = 1.1$ ) and LA4 ( $\eta = 1.5$ ) at 20 d compared with the observed spectrum of SN 1992A [5 days after maximum light (Kirshner et al. 1993)].

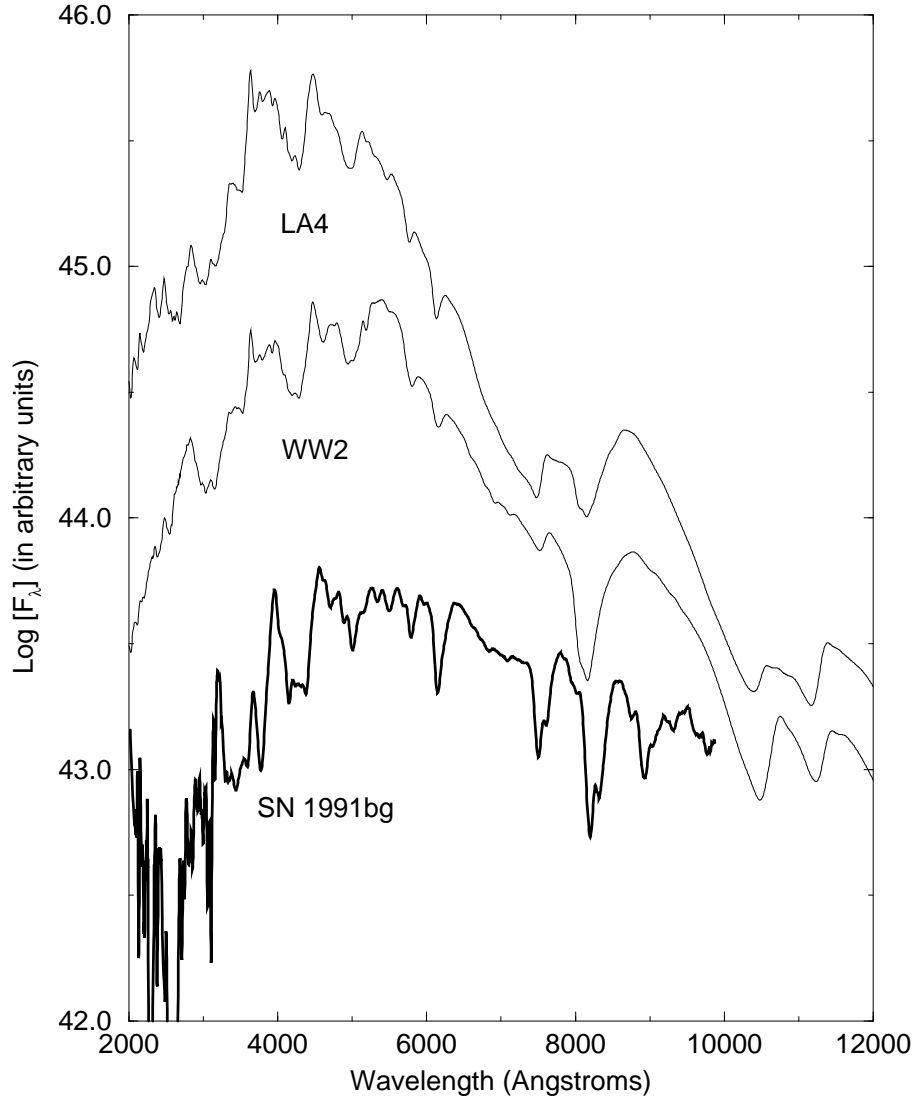


Fig. 8.— The synthetic spectra of WW2 ( $\eta = 1.1$ ) and LA4 ( $\eta = 1.5$ ) at 20 d compared with the observed spectrum of SN 1991bg [at maximum light (Filippenko et al. 1992; NASA Astrophysics Data Facility 1991)].



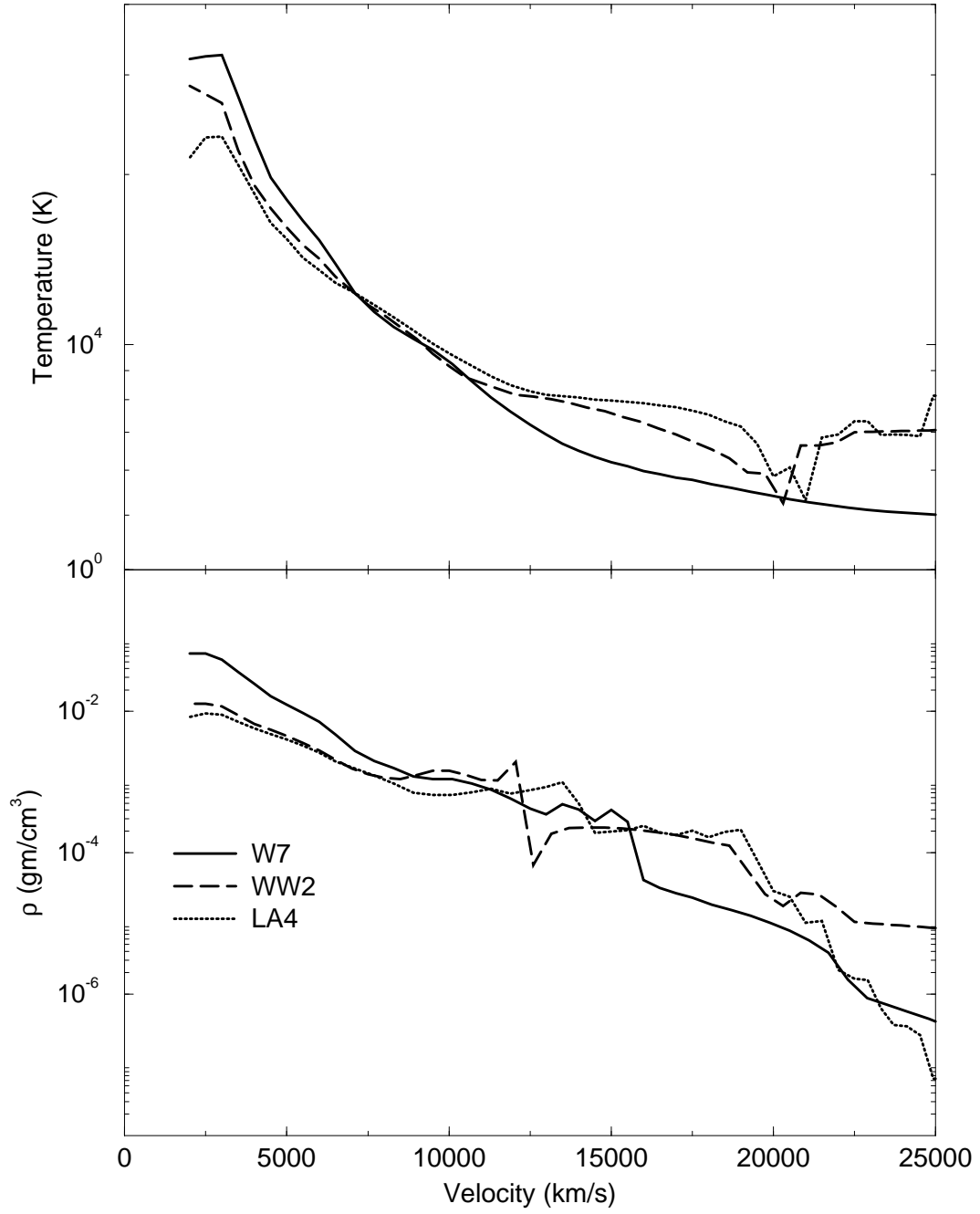


Fig. 9.— The electron density and temperature profiles for WW2 and W7 at 20 d, with  $\eta = 1.1, 1.0$  respectively. The “glitches” in the density and temperature occur at the edge of the burning fronts and represent real changes in model structure.

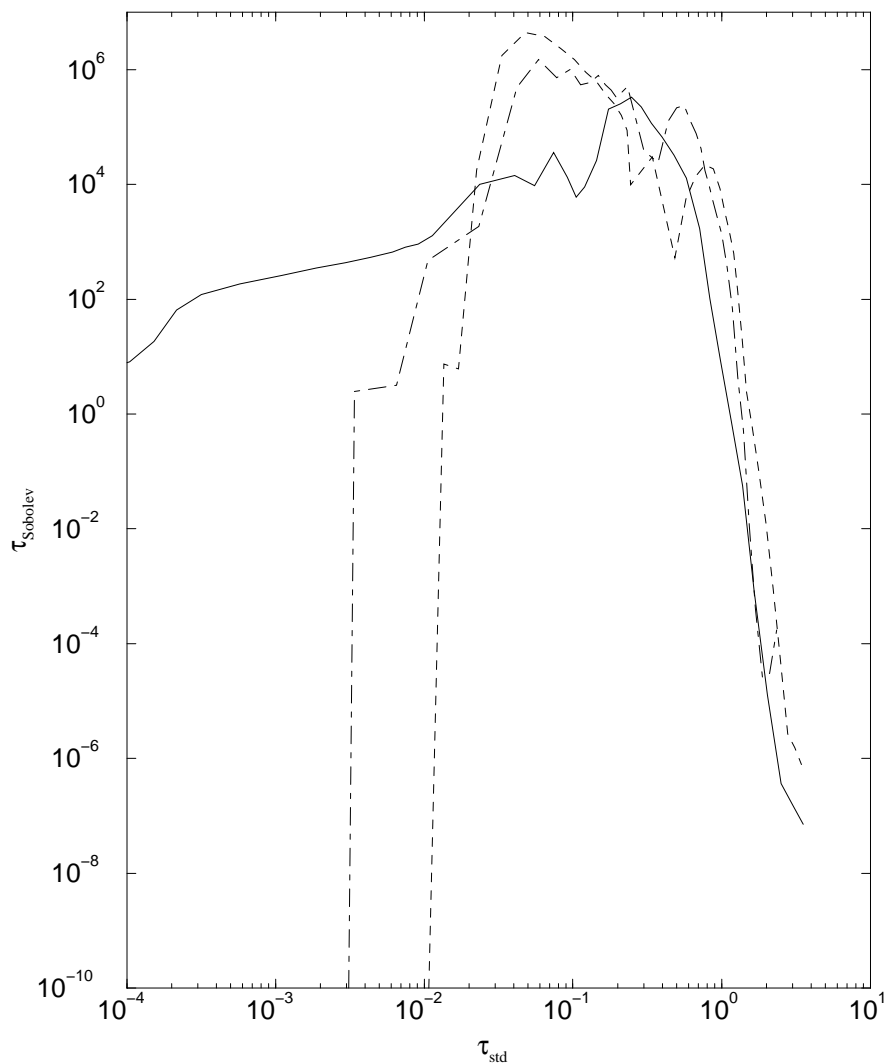


Fig. 10.— The Sobolev optical depth of the Co II  $^1D - ^3G^o$   $\lambda 2605.2$  line as a function of  $\tau_{\text{std}}$  for the 3 models listed in Table 3. The solid line denotes the W7 model, the dashed line WW2, and the dot-dashed line LA4. Note that  $\tau_{\text{Sobolev}}$  is a purely local quantity and hence is not necessarily monotonic.